Materials Chemistry and Physics 278 (2022) 125639

Contents lists available at ScienceDirect

Materials Chemistry and Physics

journal homepage: www.elsevier.com/locate/matchemphys

Preparation of MoS_2 spheres from Mo plate and elemental sulfur and the effect of sphericalization on electrochemical hydrogen evolution catalysis

Da-Som Shin, Zhenyu Jin, Seokhee Shin, Suhyun Lee, Hyeri Choi, Yo-Sep Min *

Department of Chemical Engineering, Konkuk University, 120 Neungdong-Ro, Gwangjin-Gu, Seoul, 05029, South Korea

HIGHLIGHTS

- MoS_2 spheres are synthesized from metallic Mo and elemental sulfur in hot water.
- Hydrolysis of sulfur produces H_2S and H_2SO_4 to form amorphous MoS_x spheres.
- Amorphous MoS_x spheres are transformed into crystalline MoS_2 spheres (c-MoS_2).
- The Tafel slopes of the spheres are similar to those of thin-film type catalysts.
- The sphericalization of catalyst does not affect its intrinsic activity and mechanism.

ARTICLE INFO

Keywords:
hydrothermal Synthesis
Molybdenum disulfide
MoS_2 spheres
Hydrogen evolution reaction
2D materials

ABSTRACT

The growth of MoS_2 catalysts with a controlled morphology has been actively pursued to improve the electrocatalytic activity for hydrogen evolution reaction (HER) by modifying the shape of catalysts. However, it is questionable whether changes in morphological structure affect its intrinsic activity. Here we present a facile hydrothermal synthesis of amorphous MoS_x spheres on Mo plates at 180 °C using elemental sulfur. Hydrolysis of elemental sulfur during the hydrothermal synthesis produces H_2S and H_2SO_4 in hot water. Consequently, the surface of the Mo plate is sulfurized by H_2S and dissolved by H_2SO_4 to form amorphous MoS_x spheres with diameters in the range of 0.4–0.8 μm on the Mo plate. To investigate the effect of the sphericalization of crystalline MoS_2 on its intrinsic activity for the HER, the amorphous MoS_x spheres were annealed to form crystalline MoS_2 spheres. The Tafel slopes of the amorphous MoS_x (~45 mV/dec) and crystalline MoS_2 (~103 mV/dec) spheres were similar to those of amorphous MoS_x and crystalline MoS_2 thin films, regardless of whether the shape of the catalyst was sphericalized or not. This reveals that the sphericalization cannot change the intrinsic activity and the HER mechanism on molybdenum sulfide.

1. Introduction

Molybdenum disulfide (MoS_2) has a two-dimensional (2D) layered structure due to the weak van der Waals interaction between each layer [1,2]. Since the advent of graphene, 2D materials have attracted much attention owing to their exceptional structures and excellent properties such as atomic thickness, high anisotropy, large surface-to-volume ratio, and electron confinement [3–5]. MoS_2 and graphene possess similar functional properties, including high charge carrier transport, good mechanical strength, high wear resistance, and lubrication ability [6]. Unlike graphene, which is chemically inert and has no bandgap, MoS_2, one of transition metal dichalcogenides (TMDCs), has intrinsic chemical activity and bandgap [4,7]. TMDCs in the form of MX_2, where M^{4+} and X^{2-} are transition metal cations and chalcogen anions, respectively, have a tunable bandgap [8]. Depending on the layer stacking, the bandgap of MoS_2 can be adjusted in the range of 1.3–1.8 eV. Bulk MoS_2 has an indirect bandgap of ~1.3 eV, while monolayer MoS_2 has a direct bandgap of ~1.8 eV [9]. This is advantageous for the development of optoelectronic devices, photocatalysts, and transistors [10–12].

MoS_2 has attracted attention as an electrochemical catalyst for hydrogen evolution reaction (HER) to replace platinum group metals (PGMs) [13–15]. Because the Gibbs energy change of the hydrogen adsorption on MoS_2 is close to zero, the evolution of hydrogen gas is electrochemically accelerated on active sites of MoS_2 catalyst [14–16]. It

* Corresponding author.
E-mail address: ysmin@konkuk.ac.kr (Y.-S. Min).

https://doi.org/10.1016/j.matchemphys.2021.125639
Received 16 June 2021; Received in revised form 12 October 2021; Accepted 14 December 2021
Available online 20 December 2021

is well known that the active sites of crystalline MoS_2 for the HER are the adsorption sites at the edge rather than those at the basal plane [15]. Therefore, several morphological studies have been attempted to increase the number of active edge sites of MoS_2 by morphological control. For example, MoS_2 nanoparticles were synthesized on reduced graphene oxide to increase the number of active edge sites and conductivity [17]. Various attempts to prepare alternative morphological structures such as vertically aligned or flower-like MoS_2 have been also explored to improve the catalytic activity by exposing more abundant edge sites [18,19]. Because the electrocatalytic performance is still insufficient to replace PGMs, many researchers have focused on enhancing the intrinsic catalytic activity (i.e., exchange current density and Tafel slope) of MoS_2 through several approaches such as defect-engineering [20,21], incorporation of heteroatoms [22–26], and utilization of the amorphous phase [27–30]. However, the question remains as to whether changing the morphological structure of the catalyst affects its intrinsic catalytic activity. From this point of view, it is worth investigating the synthesis of crystalline MoS_2 spheres and the effect of the sphericalization of catalysts on the intrinsic catalytic activity for the HER.

Shi et al. synthesized micro-sized MoS_2 spheres by extraction-solvothermal method to control the morphology of MoS_2 using Cyanex 301 (di-(2,4,4-trimethylpentyl) dithiophosphinic acid) as a sulfur source as well as a phase transferring and reducing agent [31]. Haruta et al. also reported a preparation method of colloidal MoS_2 spheres [32]. The MoS_2 spheres were obtained by homogeneous precipitation from a solution of ammonium orthomolybdate with thioacetamide, hydrazine, acetic acid, and ammonia. Hydrazine was used to accelerate the hydrolysis of thioacetamide to generate hydrogen sulfide.

For the preparation of crystalline MoS_2 (c-MoS_2) spheres, we present a facile hydrothermal method using Mo plates and elemental sulfur. In our hydrothermal synthesis, hydrogen sulfide (H_2S) and sulfuric acid (H_2SO_4), which play roles of sulfurizing agent and dissolving agent, respectively, are produced by hydrolysis of elemental sulfur in hot water (180 °C). The competition between the sulfurization and dissolution of the surface Mo atoms leads to the formation of amorphous MoS_x (a-MoS_x) spheres on the Mo plate. Using c-MoS_2 spheres prepared by annealing the a-MoS_x spheres, the catalytic activity of the MoS_2 spheres was investigated to answer the question of whether sphericalization of the catalyst affects the intrinsic catalytic activity for the HER.

2. Experimental

Mo plates (99.95%, 0.5 mm, Alfa Aesar) were used as a Mo precursor to synthesize molybdenum sulfide spheres on the plate. Mo powder (99.5%, 170 mesh, Alfa Aesar) was used as an alternative Mo precursor when the Mo plates were not suitable for a particular analysis such as energy dispersive spectroscopic images.

Prior to hydrothermal synthesis, Mo plates were ultrasonically cleaned with deionized water, acetone, and then ethanol (for 10 min for each solvent). For the hydrothermal process, we used an autoclave (iNexus, Inc., IN-L50) with a liner (polytetrafluoroethylene, PTFE) of which volume is 50 mL. Mo plates were cut into 1 cm × 4 cm rectangles and placed in a PTFE liner charged with 10 mmol of sulfur powder (99.98%, Sigma-Aldrich) and 30 mL of deionized water. The PTFE liner was then placed in an autoclave and heated to 180 °C for 24 h. Finally, the Mo plate was removed from the cooled autoclave, washed with deionized water, and then dried.

In the hydrothermal synthesis using Mo powder, 0.5 mmol of Mo powder was charged in a PTFE liner with 10 mmol of sulfur powder and 30 mL of deionized water. An autoclave containing Mo and S powders and water in the PTFE liner was heated to 180 °C for 12 h. All hydrothermal processes were performed by modifying the experimental procedure previously reported [33–35].

For comparison between amorphous and crystalline spheres, a plate of MoS_x/Mo prepared from Mo plates was crystallized at 1000 °C for 5 min by rapid thermal annealing (MILA-5000, ULVAC). For the annealing process, the ramp-up rate was 20 °C/s, and the working pressure was ~2.5 torr with an argon flow rate of 0.5 L/min.

Scanning electron microscopic (SEM) and energy dispersive spectroscopic (EDS) images were taken with a Field emission SEM (Hitachi SU8010). X-ray diffraction (XRD) patterns were measured using a Rigaku SmartLab diffractometer (Cu- Kα). Raman spectra were obtained using a Witech Alpha 500R spectrometer (532 nm). Photoemission spectra of X-ray photoelectron spectroscopy (XPS) were collected using a Thermo K-alpha XPS system (Al- Kα). An electron flood gun was sprayed to prevent peak shifts due to the so-called charging effect. The C 1s peak (284.8 eV) of adventitious carbon was used as an internal standard for calibrating the binding energy.

Electrochemical measurements were performed using a potentiostat (Biologic, SP-150) with a typical three electrodes setup in a solution of 0.5 M H_2SO_4. A Hg/Hg_2SO_4 (K_2SO_4 saturated) electrode and a graphite rod were used as reference and counter electrodes, respectively. The plates of a-MoS_x/Mo and c-MoS_2/Mo were used as a working electrode. The geometric area (1 cm × 1 cm) of the plate for electrochemical measurements was defined with a Kapton tape as previously reported [29]. The reference electrode was calibrated to the reversible hydrogen potential using Pt wires for both the working and counter electrodes in the same solution of 0.5 M H_2SO_4 under H_2 gas purge. According to the calibration, the electrochemical potential difference between the reversible hydrogen electrode (RHE) and the reference electrode (Hg/Hg_2SO_4) is given by $E(RHE) = E(Hg/Hg_2SO_4) + 0.704$ V. Polarization curves for HER were obtained using linear sweep voltammetry (LSV) over the potential range of +0.1 V to −0.4 V vs RHE. The series resistance of the electrochemical cell before each LSV was determined by electrochemical impedance measurement performed at an open circuit potential with an AC amplitude of 25 mV while scanning the frequency from 200 kHz to 50 mHz. The series resistances of the working electrodes were measured to be ~1.31 Ω for as-received Mo plates, ~2.39 Ω for bare Mo plates (annealed at 1000 °C), 3.05 Ω for a-MoS_x/Mo, and 1.52 Ω for c-MoS_2/Mo (annealed at 1000 °C). See Fig. S1 for the Nyquist plot of each working electrode. The Ohmic potential drop (*iR*) losses were corrected using the series resistances obtained from the electrochemical impedance measurement. A stability test was performed by repeating a cyclic voltametric (CV) scan in the potential range of +0.1 V to −0.4 V vs RHE with a scan rate of 50 mV/s with a Pt counter electrode.

3. Results and discussion

In the hydrothermal method using Mo plates and elemental sulfur, molybdenum sulfide spheres are synthesized at 180 °C by hydrolysis of sulfur in the presence of the Mo plate (or Mo powder). Fig. 1 shows FE-SEM images of the spheres hydrothermally synthesized from Mo plate (Fig. 1a) and Mo powder (Fig. 1b). The diameter of the spheres ranges from 0.4 to 0.8 μm regardless of the type of Mo source. The average diameter of spheres was around 0.61 μm with a standard deviation of ±0.08 μm (see the histogram in Fig. 1a).

Oana and Ishikawa reported that elemental sulfur and water react to form hydrogen sulfide (H_2S) and sulfuric acid (H_2SO_4) at high temperature (150–300 °C) in an autoclave [36] via hydrolysis of sulfur:

$$4S + 4H_2O \rightarrow 3H_2S + H_2SO_4$$

Maldonado-Zagal and Boden also reported that hydrolysis of sulfur in hot water consists of the disproportionation of the octa-atomic sulfur (S_8) into oxidized (S^{2-} of H_2S) and reduced (S^{6+} of H_2SO_4) compounds [33]. According to their estimation performed over a wide range of temperatures (15–288 °C), the activation energy for hydrolysis of sulfur in water is in the range of 40–52 kJ/mol. Ellis and Giggenbach investigated the effects of temperature and pressure on the hydrolysis of sulfur [37]. The temperature has such a large effect that the concentration of H_2S in equilibrium with molten sulfur increases by about 100

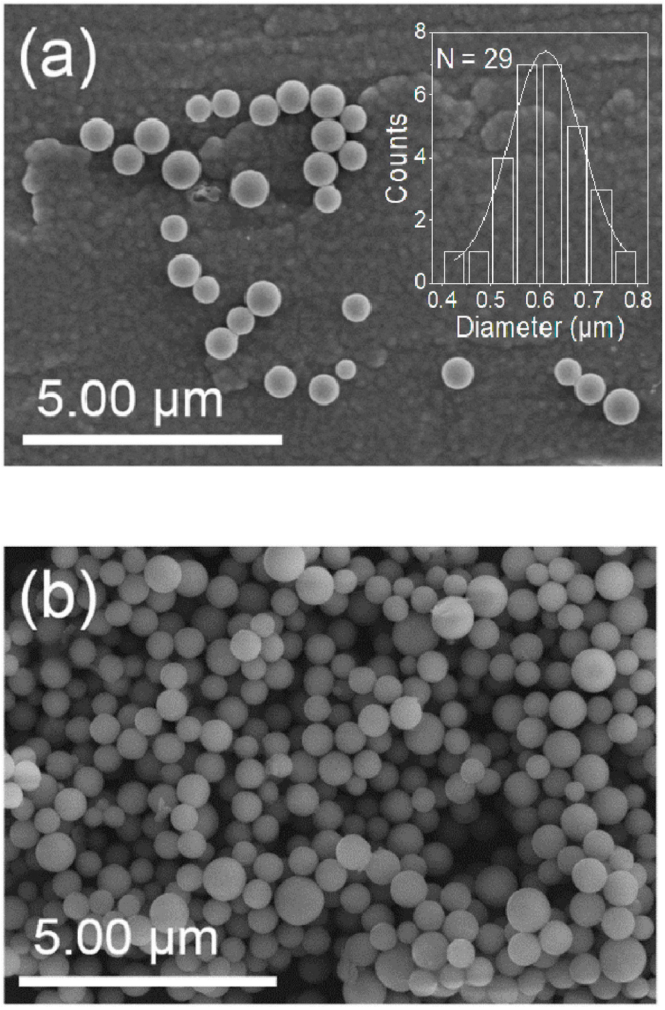

Fig. 1. FE-SEM images of a-MoS_x spheres synthesized from Mo plate (a) and Mo powder (b) by hydrothermal synthesis.

times between 100 and 300 °C. In comparison, the pressure effect on hydrolysis is minor.

During our hydrothermal process, H_2S generated by the hydrolysis sulfurizes the Mo plate (or the Mo powder). Furthermore, H_2SO_4 dissolves non-sulfurized Mo atoms to form the MoS_x spheres, because hot H_2SO_4 solution dissolves metallic molybdenum [38]. Consequently, H_2SO_4 contributes to the formation of MoS_x spheres on the Mo plate by dissolving the non-sulfurized Mo atoms near the sulfurized MoS_x domain.

After the hydrothermal synthesis, the smell of the solution was reminiscent of rotten eggs, and the pH of the solution was approximately 2.0 or less in both Mo plate and powder experiments. This is evidence that the hydrolysis of sulfur powder produces H_2S and H_2SO_4 as previously reported [33,36,37]. To clearly understand the role of H_2S, we performed another hydrothermal process of Mo plate in 0.5 M H_2SO_4 solution without elemental sulfur. However, no spherical particles were found in the FE-SEM image (Fig. S2) after performing the hydrothermal process without sulfur powder. This reveals that H_2SO_4 alone cannot produce MoS_x spheres but H_2S plays a critical role in the formation of MoS_x spheres.

To identify the composition of the spheres, we tried to obtain EDS mapping images of the spheres synthesized from a Mo plate. However, clear EDS mapping images of the spheres could not be obtained because two EDS peaks of Mo (Lα: 2.293 keV) and S (Kα: 2.307 eV) were not resolved and the substrate was also Mo plate (Fig. S3). As an alternative way, a dispersion solution of spheres was taken from a solution hydrothermally processed with Mo powder (see the experimental section). The dispersion solution was dropped on a silicon wafer and dried to obtain EDS mapping images. Fig. 2(b–d) show the mapping images of Mo (Lα), S (Kα), and O (Kα) EDS peaks obtained in the same region of the SEM image (Fig. 2a). The spheres mainly consist of Mo and S atoms as the spherical shapes are visible in the mapping images of the Mo and S peaks (Fig. 2b and c). However, the image of the O peak (Fig. 2d) is noisy due to its low concentration.

The as-synthesized molybdenum sulfide spheres on the Mo plate are characterized to be amorphous in XRD pattern (black line in Fig. 3) in which there is no crystalline MoS_2 peak and only metallic Mo peaks (black squares) are observed from the Mo plate (JCPDS 01–1208). After annealing the amorphous MoS_x (a-MoS_x) at 1000 °C for 5 min in Ar atmosphere, the annealed spheres were crystallized to the 2H-structure of molybdenite (c-MoS_2) as indicated by the presence of a strong peak at $2\theta = 14.28°$ (blue diamond) in Fig. 3 (blue line). The peak is attributed to the (002) basal planes of the 2H structure and the interplanar spacing (d_{002}) is calculated to be ~0.619 nm, which is in good agreement with that (0.615 nm) of molybdenite [39]. However, since the crystal faces were well developed by annealing, the surface of the c-MoS_2 spheres was bumpy due to the presence of the crystal facets as shown in the FE-SEM image (Fig. 4).

In Fig. 5, the Raman spectrum of the annealed spheres also supports the presence of the 2H structure of MoS_2 in the c-MoS_2/Mo plate. The characteristic E^1_{2g} (in-plane) and A_{1g} (out-of-plane) vibrational modes of molybdenite appear at ~383.7 and ~409.5 cm^{-1}, respectively. These values well agree with the E^1_{2g} (383 $cm^{-1} \pm 1$) and A_{1g} (409 $cm^{-1} \pm 1$) peaks of bulk MoS_2 previously reported [40]. Moreover, the strongest A_{1g} peak of c-MoS_2 spheres is so narrow with a full width at half-maximum (FWHM) of ~6.1 cm^{-1} owing to its high crystallinity [41,42].

On the other hand, the E^1_{2g} and A_{1g} bands in the as-synthesized spheres (a-MoS_x/Mo plate) are very weak, and several peaks of elemental sulfur (black triangles) are observed in the spectrum, due to the presence of sulfur residues after the hydrothermal process [43]. However, the specimen of c-MoS_2 is free of sulfur residues in the Raman spectrum owing to the evaporation of sulfur during the annealing process performed in a vacuum (~2.5 torr).

For the as-synthesized MoS_x spheres, the characteristic vibration modes (blue diamonds) of E^1_{2g} and A_{1g} weakly appear at ~380.0 and ~404.6 cm^{-1}, although its phase is amorphous in XRD. There are several reports on the appearance of weak vibrational bands of E^1_{2g} and A_{1g} in amorphous MoS_x particles and thin films [30,41,44]. In general, the peaks of the amorphous phase show significant red-shift and broadening compared to those of the crystalline phase. Indeed, the A_{1g} peak of a-MoS_x spheres is red-shifted by ~4.9 cm^{-1} with a wide FWHM of ~10 cm^{-1}.

XPS analyses were performed on the a-MoS_x/Mo and c-MoS_2/Mo plates to determine the chemical state of the spheres and the stoichiometric ratios of Mo and S. All binding energies were calibrated with the C 1s peak (284.8 eV) of adventitious carbon.

In Fig. 6a, the doublet of Mo 3d peaks of a-MoS_x appears at binding energies of 229.5 eV (Mo^{4+} $3d_{5/2}$) and 232.7 eV (Mo^{4+} $3d_{3/2}$), indicating the presence of Mo^{4+} ions [41,45,46]. Note that the doublet of Mo 3d shifts to higher binding energies for the higher oxidation states of Mo^{5+} and Mo^{6+} [26,46]. The large S 2s peak at 227.9 eV overlaps with the Mo $3d_{5/2}$ peak. This reveals that there are not only divalent sulfide ions (S^{2-}) but also other sulfur components such as monovalent sulfur (S_2^{2-}), sulfate (SO_4^{2-}), and elemental sulfur (S^0) residues. In Fig. 6b, the S 2p peak of the sulfate appears at ~168.5 eV with high binding energy due to its high oxidation state (S^{6+}) [45].

For the binding energies of the S 2p peaks of a-MoS_x in Fig. 6b, the S $2p_{1/2}$ peak (164.8 eV) is not resolved but appears as a shoulder of the $2p_{3/2}$ peak (163.6 eV) as previously reported for amorphous MoS_x [41]. Using the deconvoluted spectra in Figs. S4(a–c), the ratio of S/Mo is estimated to be ~7.7, indicating the presence of a considerable amount

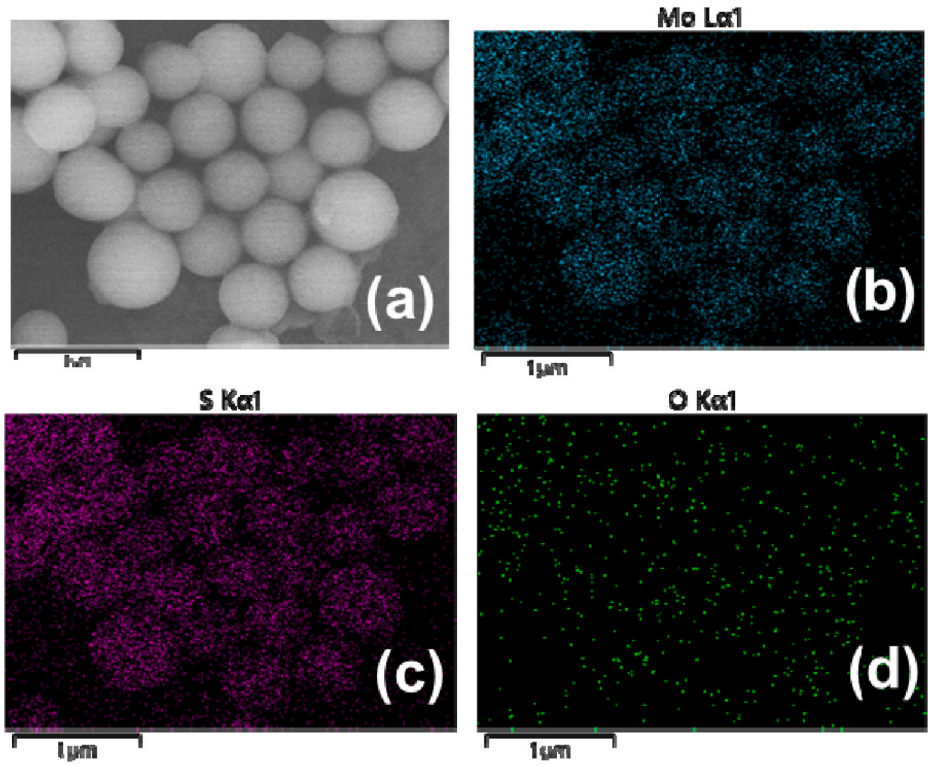

Fig. 2. SEM image (a) and EDS mapping Images (b–d) of a-MoS_x spheres on a silicon wafer: (a) SEM image, (b) Mo peak (Lα: 2.293 keV), (c) S peak (Kα: 2.307 keV), (d) O peak (Kα: 0.525 keV). (For interpretation of the references to colour in this figure legend, the reader is referred to the Web version of this article.)

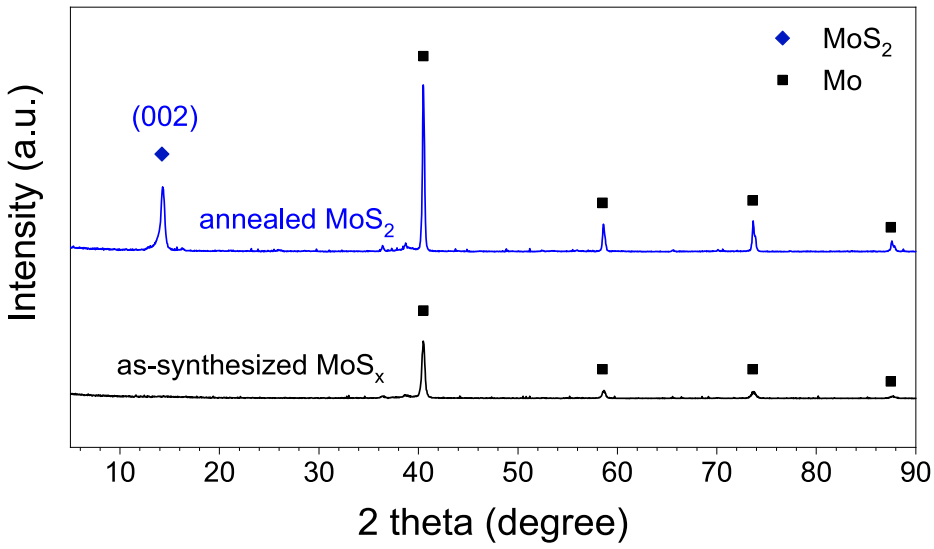

Fig. 3. XRD patterns of molybdenum sulfide spheres on Mo plate: as-synthesized a-MoS_x (black) and annealed c-MoS_2 (blue). (For interpretation of the references to colour in this figure legend, the reader is referred to the Web version of this article.)

of elemental sulfur residue (see Table S1). In addition, an amount of oxygen (17.6%), which originated from sulfate (SO_4^{2-}, 4.6%), is also observed. The theoretical ratio of O^{2-} to S^{6+} in sulfate is 4. Indeed, the estimated ratio of O^{2-} to S^{6+} from the deconvoluted spectra (Fig. S4b) is around 3.8. This also supports that the oxygen observed in a-MoS_x is attributed to the presence of sulfate.

For the c-MoS_2 specimen (Fig. 6c), the presence of Mo^{4+} can be seen as clearly resolved peaks at binding energies of 229.8 eV (Mo^{4+} $3d_{5/2}$) and 232.9 eV (Mo^{4+} $3d_{3/2}$) [41,45,46]. The S 2s peak (227.1 eV) of c-MoS_2 is resolved from the Mo $3d_{5/2}$ peak and much smaller than that of a-MoS_x due to the evaporation of residual sulfur during the annealing process. The binding energies of the divalent sulfide ion (S^{2-}) of c-MoS_2 (Fig. 6d) are also clearly resolved into the $2p_{3/2}$ peak at 162.6 eV and the $2p_{1/2}$ peak at 163.8 eV. Furthermore, the ratio of S/Mo is estimated to be ~2.0 from the deconvoluted spectra (Fig. S4), as expected for c-MoS_2 (Table S1).

To investigate the catalytic activity of the MoS_2 spheres, a-MoS_x/Mo plates or c-MoS_2/Mo plates were used as working electrodes for hydrogen evolution. The *iR*-corrected polarization curves (Fig. 7) were obtained by linear sweep volumetric measurements in 0.5 M H_2SO_4 solution using a typical three-electrode setup. The HER activities of as-received Mo and annealed Mo plates (1000 °C) were also investigated

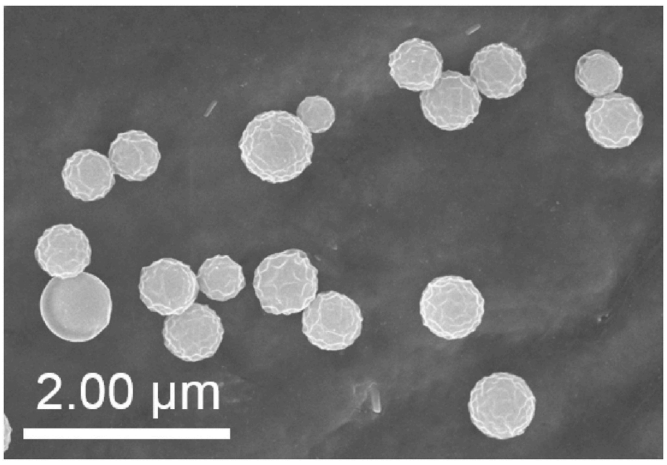

Fig. 4. FE-SEM image of c-MoS_2 spheres prepared by annealing a-MoS_x spheres at 1000 °C for 5 min under Ar atmosphere.

in the same way for comparison. The cathodic current density of a-MoS_x/Mo (blue solid line) is significantly lower than those of amorphous MoS_x catalysts previously reported [27–30,44]. The cathodic current density of a-MoS_x/Mo is ~1.10 mA/cm^2 at an overpotential of 250 mV, while the previously reported amorphous thin films of MoS_x catalysts exhibit a current density of ~10 mA/cm^2 in the overpotential range of 200–300 mV [29,44]. Even the as-received Mo plate without hydrothermal and annealing processes reaches a current density of 0.74 A/cm^2 at 250 mV. Furthermore, the cathodic current density of c-MoS_2/Mo is much lower than that of a-MoS_x/Mo. However, this simple comparison of the cathodic current densities is unfair because the a-MoS_x or c-MoS_2 spheres sparsely cover the surface of the plates as shown in Fig. 1a. Note that the cathodic current is divided by the geometric area of the electrode to obtain the current density. Consequently, the cathodic current density is underestimated for the spheres sparsely covered on the surface.

As is well known, the cathodic current density (j) in the polarization curve of HER can be related to the overpotential (η) by the Tafel equation, $\eta = a + b \log j$, where b is the Tafel slope [47]. From the slope and intercept of the semilogarithmic plot (Fig. 8) of $\log j$ against η (so-called Tafel plot), the Tafel slope (b) and the exchange current density (j_0) can be estimated, respectively, as listed in Table 1. Regarding the exchange current density (j_0) and Tafel slope (b), which represent the intrinsic activity of the catalyst, it is required to reach higher values of j_0 and lower values of b to achieve the high performance of the catalyst.

Generally, the Tafel slope depends on the HER mechanism and the exchange current density is related to the catalytic activity at the equilibrium of HER. However, the j_0 values listed in Table 1 are also not suitable for comparison with each other, due to the rare presence of a-MoS_x (or c-MoS_2) spheres (see SEM image of Fig. 1a) and the presence of residual sulfur on the surface of a-MoS_x/Mo (see Raman spectrum of Fig. 5 and XPS spectrum of Fig. 6a).

The Tafel slope (b) is the slope of the linear region on the Tafel plot. Thus, it represents the overpotential required to increase the current density by one order of magnitude. Therefore, the b value still provides useful information for the HER mechanism because it is not determined from the absolute value of current density, but from the relative change in the current density by increasing the overpotential.

According to the classical kinetic theory of HER in acidic media, there are three possible reaction steps: Volmer reaction (discharge step: $H_3O^+ + e^- \rightarrow H_{ads} + H_2O$), Tafel reaction (catalytic recombination step: $H_{ads} + H_{ads} \rightarrow H_2$), and Heyrovsky reaction (electrochemical desorption step: $H_{ads} + H_3O^+ + e^- \rightarrow H_2 + H_2O$) [29,47]. Because the Volmer reaction for electrochemical adsorption of hydrogen on the active site should be followed by the Tafel reaction or Heyrovsky reaction for the evolution of hydrogen gas, there are two pathways for HER: Volmer-Tafel (VT) and Volmer-Heyrovsky (VH) mechanisms. Depending on which step is the rate-determining step (rds), the theoretical Tafel slopes of $\overline{V}T$, $V\overline{T}$, $\overline{V}H$, and $V\overline{H}$ mechanisms are 120, 30, 120, and 40 mV/dec, respectively (the bar denotes the rds).

Most amorphous MoS_x catalysts, prepared by various methods such as electrochemical deposition [27], wet chemical synthesis [28], hydrothermal deposition [48], and atomic layer deposition [29,44], exhibit Tafel slopes in the range of 40 − 50 mV/dec. Similarly, the Tafel slope of a-MoS_x/Mo is ~45 mV/dec, as shown in Fig. 8 and Table 1. This value, close to the theoretical value of the $V\overline{H}$ mechanism (40mV/dec), indicates that the hydrogen evolution on a-MoS_x spheres follows the Volmer-Heyrovsky mechanism ($V\overline{H}$) like other amorphous MoS_x thin films. Therefore, the rds of HER on the a-MoS_x sphere is the Heyrovsky reaction in which a proton approaches the adsorbed hydrogen atom to produce hydrogen gas through electrochemical desorption. Recently, Yeo, et al. confirmed the participation of S atoms as catalytically active

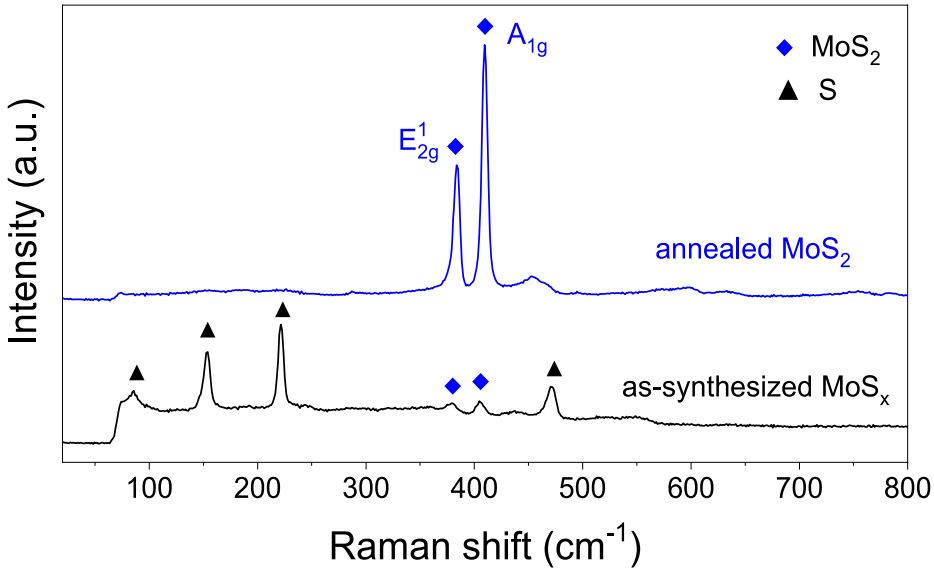

Fig. 5. Raman spectra of a-MoS_x (black) and c-MoS_2 (blue). (For interpretation of the references to colour in this figure legend, the reader is referred to the Web version of this article.)

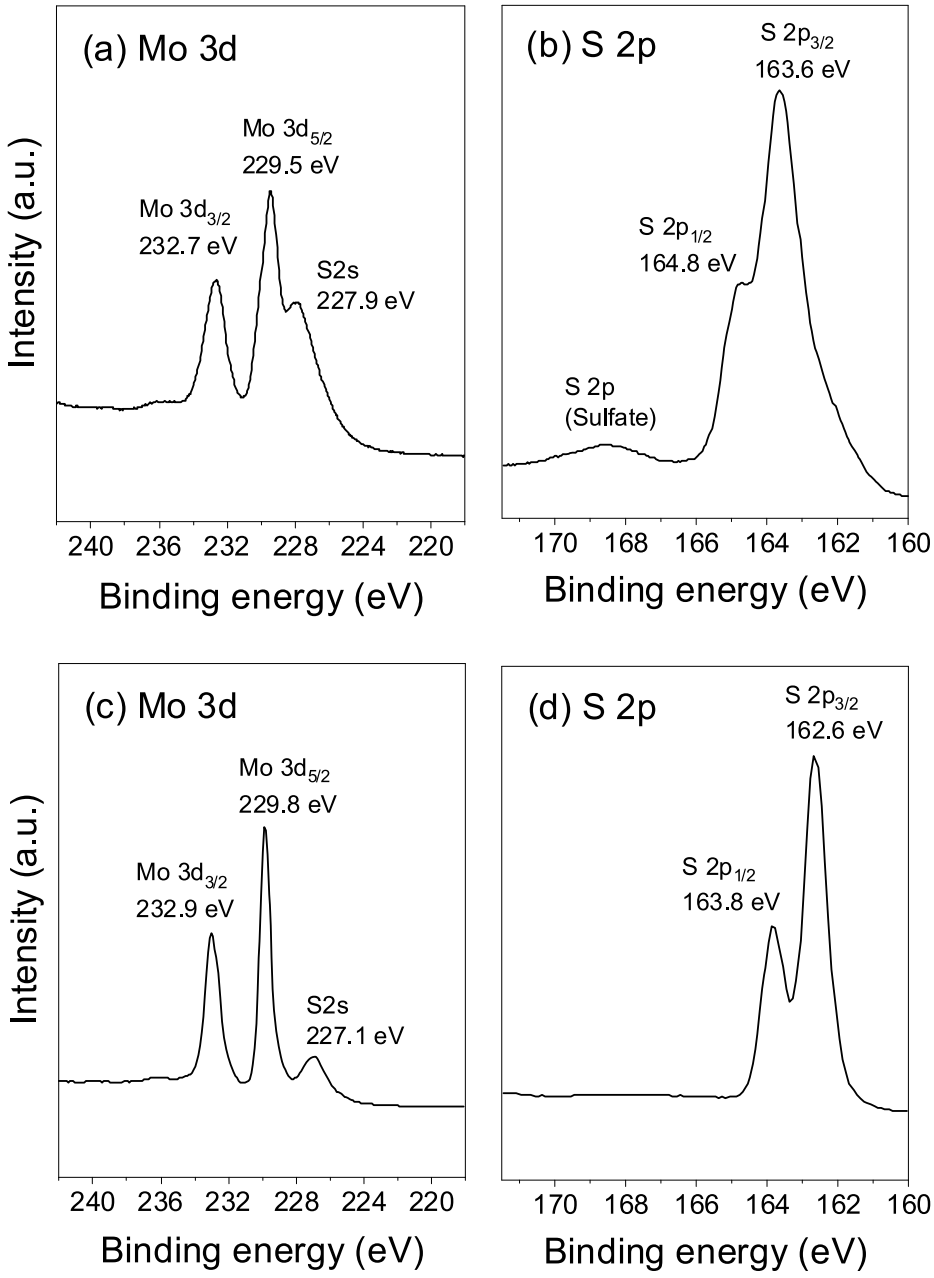

Fig. 6. XPS spectra of (a, b) a-MoS_x and (c, d) c-MoS_2 spheres.

sites for hydrogen evolution on a-MoS_x films using operando Raman spectroscopic analysis [49]. However, despite considerable efforts, elucidating the active site of proton reduction on amorphous MoS_x catalyst still remains elusive, because the sulfur atoms of the amorphous catalysts exist in various chemical states such as bridging S_2^{2-}, terminal S_2^{2-}, unsaturated S^{2-}, and apical S^{2-} [50].

The Tafel slope of c-MoS_2/Mo is ~103 mV/dec, rather close to the theoretical value (120 mV/dec) of the $\overline{V}T$ or $\overline{V}H$ mechanisms. This reveals that the rds of HER on c-MoS_2 spheres is the Volmer reaction (discharge step) in which protons are converted to adsorbed hydrogen atoms on the catalyst surface. The crystalline bulk MoS_2 has a high Tafel slope (~692 mV/dec) due to the lack of exposed edge sites and the large internal resistance attributed to its semiconducting nature [51]. However, the Tafel slope of c-MoS_2 spheres (~103 mV/dec) is rather similar to that of vertically aligned crystalline MoS_2 thin films (105 – 120 mV/dec) rich in catalytically active edge sites [18]. The lack of significant difference in the Tafel slope between the c-MoS_2 spheres and the vertically aligned thin films suggests that simply changing the morphological structure of the catalyst does not affect the intrinsic catalytic activity since the HER still follows the same mechanism.

The as-received Mo plate and the annealed Mo plate were also investigated as a control sample for a-MoS_x/Mo plate and c-MoS_2/Mo plate, respectively. The exchange current densities of the as-received Mo plate and the annealed Mo plate are consistent with the j_0 values (0.050–0.355 μA/cm^2) reported by Pentland et al. [52]. The Tafel slopes of the as-received Mo plate (64 mV/dec) and the annealed Mo plate (80 mV/dec) are significantly different from each other due to the high temperature (1000 °C) annealing. As shown in Fig. 9, the crystal structure of the as-received Mo plate with a preferential orientation of the (110) plane is transformed into a polycrystalline structure with random orientations during the annealing. Pentland et al. also reported a Tafel slope of 78 mV/dec for Mo treated at high temperature (2200 °C), suggesting a rate-determining electrochemical desorption mechanism on the Mo electrode [52].

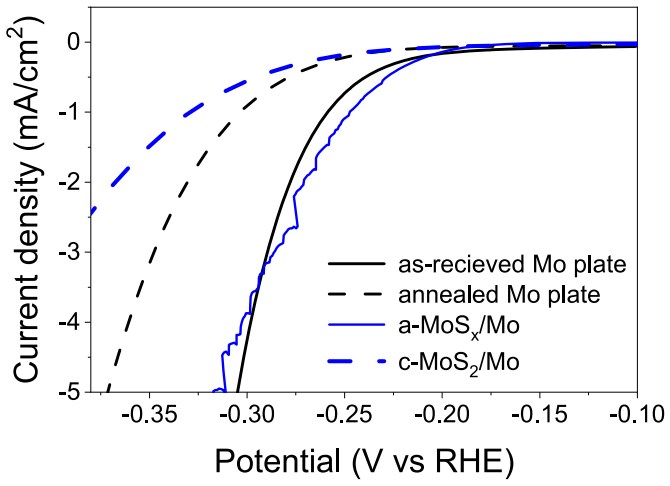

Fig. 7. *iR*-corrected polarization curves of as-received Mo plate, annealed Mo plate, a-MoS_x/Mo, and c-MoS_2/Mo.

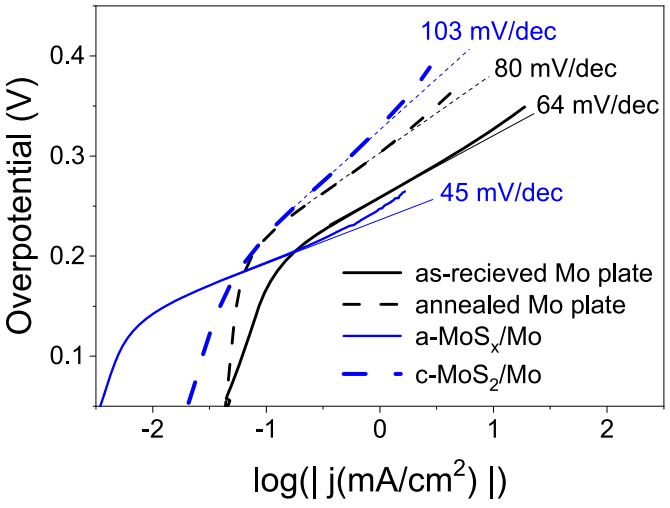

Fig. 8. Tafel plots of as-received Mo, annealed Mo, a-MoS_x/Mo, and c-MoS_2/Mo plates.

Table 1
Electrochemical characteristics of as-received Mo, annealed Mo, a-MoS_x/Mo, and c-MoS_2/Mo plates.

Working electrode	Tafel slope (mV/dec)	j_0 (μA/cm^2)
as-received Mo	64	0.091
annealed Mo	80	0.163
a-MoS_x/Mo	45	0.005
c-MoS_2/Mo	103	0.679

Although the stability of HER catalysts is one of the major issues for industrial applications, it is difficult to estimate the intrinsic stability of the catalyst spheres due to the separation of the spheres from the Mo plate during the stability test (see SEM images of Fig. S5). However, contrary to the concerns about the detachment of the catalyst spheres, the cathodic current density increases during repeated CV scans for the stability test (Fig. 10). While the current density of the c-MoS_2/Mo catalyst slightly increases after 1000 cycles, the current density of the a-MoS_x/Mo catalyst tends to dramatically increase with the number of CV cycles. Although further research is needed to elucidate the cause, it is inferred that the increase in cathodic current density is attributed to the formation of a-MoS_x film by electrochemical reduction and oxidation of

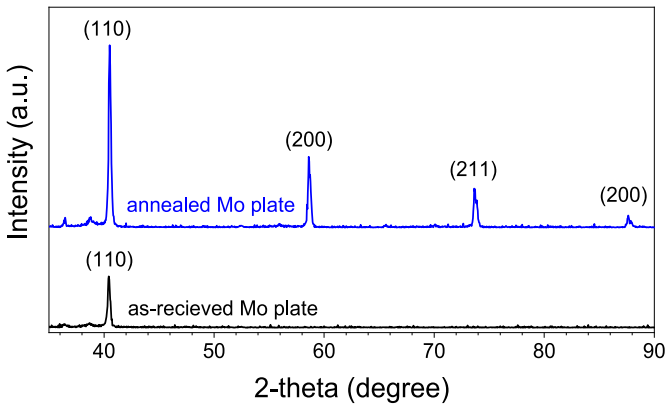

Fig. 9. XRD patterns of as-received Mo plate and annealed Mo plate (1000 °C).

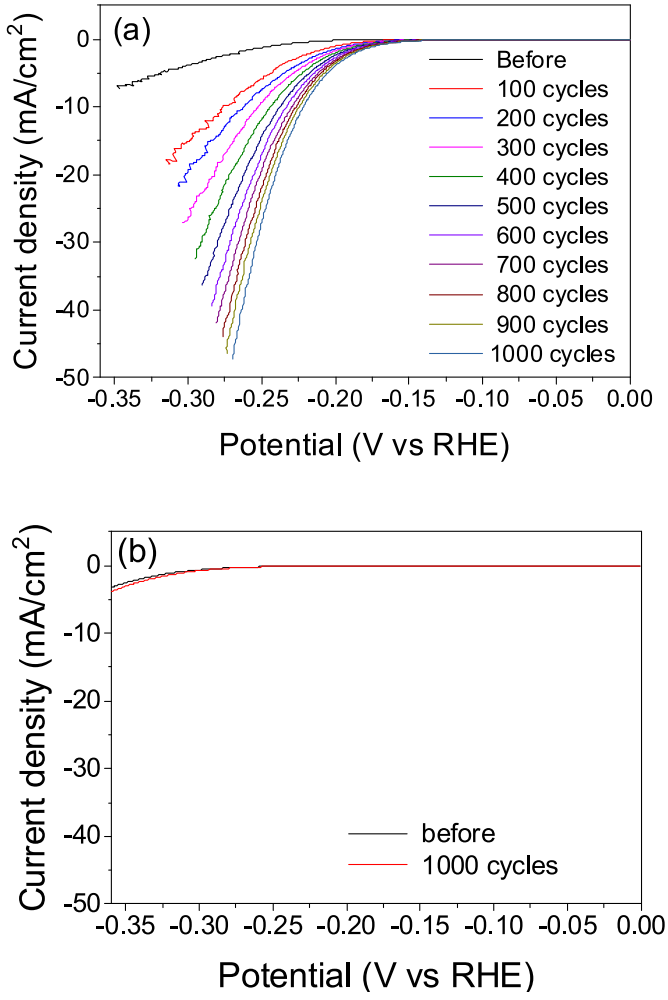

Fig. 10. Polarization curves of a-MoS_x/Mo (a) and c-MoS_2/Mo (b) catalysts before and after stability test (1000 cycles).

residual sulfur and Mo plate, respectively. This inference is supported by the XPS spectra of the catalysts after the stability test (Fig. S6) in which the sulfur 2s peaks of both catalysts were reduced in comparison to the Mo 3d peaks (Figs. S6a and S6c). Furthermore, the doublet of S 2p of c-MoS_2 should be clearly resolved as shown in Fig. 6d, but not resolved in Fig. S6d after the stability test due to the a-MoS_x formation.

4. Conclusions

Molybdenum sulfide spheres were synthesized via a facile hydrothermal method of sulfurizing a Mo plate in water under the presence of elemental sulfur. In the hydrothermal sulfurization, H_2S and H_2SO_4 generated by the hydrolysis of sulfur give rise to the formation of amorphous a-MoS_x spheres with diameters of 0.4–0.8 μm on the Mo plate. By thermal annealing, the a-MoS_x spheres were transformed into crystalline c-MoS_2 spheres with the 2H structure of molybdenite. Considering that the Tafel slopes of the a-MoS_x (~45 mV/dec) and c-MoS_2 (~103 mV/dec) spheres are similar to the previously reported Tafel slopes of the film-type catalysts of a-MoS_x and c-MoS_2, the sphericalization of the morphological structure does not affect the hydrogen evolution mechanism of the molybdenum sulfide catalyst. In addition, the facile hydrothermal synthesis may enable and facilitate the induction of spherical shape in the syntheses of various sulfide particles.

CRediT authorship contribution statement

Da-Som Shin: Writing – original draftwriting-original draft, preparation, Conceptualizationconceptualization, Investigationinvestigation. **Zhenyu Jin:** Validationvalidation. **Seokhee Shin:** Visualizationvisualization. **Suhyun Lee:** Formal analysisformal analysis. **Hyeri Choi:** Resourcesresources. **Yo-Sep Min:** Supervisionsupervision, Writing – review & editingingand.

Declaration of competing interest

The authors declare that they have no known competing financial interests or personal relationships that could have appeared to influence the work reported in this paper.

Acknowledgments

This work was supported by Konkuk University in 2017.

Appendix A. Supplementary data

Supplementary data to this article can be found online at https://doi.org/10.1016/j.matchemphys.2021.125639.

References

[1] A.B. Kaul, Two-dimensional layered materials: structure, properties, and prospects for device applications, J. Mater. Res. 29 (3) (2014) 348–361.
[2] K.S. Novoselov, D. Jiang, F. Schedin, T.J. Booth, V.V. Khotkevich, S.V. Morozov, A. K. Geim, Two-dimensional atomic crystals, Proc. Natl. Acad. Sci. Unit. States Am. 102 (30) (2005) 10451–10453.
[3] K.S. Novoselov, A.K. Geim, S.V. Morozov, D. Jiang, Y. Zhang, S.V. Dubonos, I. V. Grigorieva, A.A. Firsov, Electrical field effect in atomically thin carbon films, Science 306 (2004) 666–669.
[4] H. Zhang, M. Chhowalla, Z. Liu, 2D nanomaterials: graphene and transition metal dichalcogenide, Chem. Soc. Rev. 47 (2018) 3015–3017.
[5] S.-Y. Cho, Y. Lee, H.-J. Koh, H. Jung, J.-S. Kim, H.-W. Yoo, J. Kim, H.-T. Jung, Superior chemical sensing performance of black phosphorus: comparison with MoS2 and graphene, Adv. Mater. 28 (2016) 7020–7028.
[6] J. Theerthagiri, R.A. Senthil, B. Senthilkumar, A.R. Polu, J. Madhavan, M. Ashokkumar, Recent advances in MoS_2 nanostructured materials for energy and environmental applications-a review, J. Solid State Chem. 252 (2017) 43–71.
[7] X. Li, H. Zhu, Two-dimensional MoS_2: properties, preparation, and applications, J. Mater. 1 (2015) 33–44.
[8] W. Choi, N. Choudhary, G.H. Han, J. Park, D. Akinwande, Y.H. Lee, Recent development of two-dimensional transition metal dichalcogenides and their applications, Mater. Today 20 (3) (2017) 116–130.
[9] K.F. Mak, C. Lee, J. Hone, J. Shan, T.F. Heinz, Atomically thin MoS_2: a new direct-gap semiconductor, Phys. Rev. Lett. 105 (2010) 136805.
[10] H.L. Zhuang, R.G. Hennig, Computational search for single-layer transition-metal dichalcogenide photocrystals, J. Phys. Chem. C 117 (2013) 20440–20445.
[11] H.-M. Li, D.-Y. Lee, M.S. Choi, D. Qu, X. Liu, C.-H. Ra, W.J. Yoo, Metal-semiconductor barrier modulation for high photoresponse in transition metal dichalcogenide field effect transistors, Sci. Rep. 4 (2015) 4041.
[12] E. Singh, K.S. Kim, G.Y. Yeom, H.S. Nalwa, Two-dimensional transition metal dichalcogenide-based counter electrodes for dye-sensitized solar cells, RSC Adv. 7 (2017) 28234–28249.
[13] A.B. Laursen, S. Kegnaes, S. Dahl, I. Chorkendorff, Molybdenum sulfides-efficient and viable materials for electro- and photoelectrocatalytic hydrogen evolution, Energy Environ. Sci. 5 (2) (2012) 5577–5591.
[14] B. Hinneman, P.G. Moses, J. Bonde, K.P. Jorgensen, J.H. Nielsen, S. Horch, I. Chorkendorff, J.K. Norskov, Biomimetic hydrogen evolution: MoS_2 nanoparticles as catalyst for hydrogen evolution, J. Am. Chem. Soc. 127 (15) (2005) 5308–5309.
[15] T.F. Jaramillo, K.P. Jorgensen, J. Bonde, J.H. Nielsen, S. Horch, I. Chorkendorff, Identification of active edge sites for electrochemical H_2 evolution from MoS_2 nanocrystals, Science 317 (2007) 100–102.
[16] S.S. Chou, N. Sai, P. Lu, E.N. Coker, S. Liu, K. Artyushkova, T.S. Luk, B. Kaehr, C. J. Brinker, Understanding catalysis in a multiphasic two-dimensional transition metal dichalcogenide, Nat. Commun. 6 (2015) 8311.
[17] Y. Li, H. Wang, L. Xie, Y. Liang, G. Hong, H. Dai, MoS_2 nanoparticles grown on graphene: an advanced catalyst for the hydrogen evolution reaction, J. Am. Chem. Soc. 133 (2011) 7296.
[18] D. Kong, H. Wang, J.J. Cha, M. Pasta, K.J. Koski, J. Yao, Y. Cui, Synthesis of MoS_2 and $MoSe_2$ films with vertically aligned layers, Nano Lett. 13 (3) (2013) 1341–1347.
[19] F.Z. Wang, M.J. Zheng, B. Zhang, C.Q. Zhu, Q. Li, L. Ma, W.Z. Shen, Ammonia intercalated flower-like MoS_2 nanosheet film as electrocatalyst for high efficient and stable hydrogen evolution, Sci. Rep. 6 (2016) 31092.
[20] G. Ye, Y. Gong, J. Lin, B. Li, Y. He, S.T. Pantelides, W. Zhou, R. Vajtai, P.M. Ajayan, Defects engineered monolayer MoS_2 for improved hydrogen evolution reaction, Nano Lett. 16 (2016) 1097–1103.
[21] Q. Xu, Y. Liu, H. Jiang, Y. Hu, H. Liu, C. Li, Unsaturated sulfur edge engineering of strongly coupled MoS_2 nanosheet-carbon macroporous hybrid catalyst for enhanced hydrogen generation, Adv. Energy Mater. 9 (2019) 1802553.
[22] D. Merki, H. Vrubel, L. Rovelli, S. Fierro, X. Hu, Fe, Co, and Ni ions promote the catalytic activity of amorphous molybdenum sulfide films for hydrogen evolution, Chem. Sci. 3 (8) (2012) 2512–2525.
[23] J. Deng, H. Li, J. Xiao, Y. Tu, D. Deng, H. Yang, H. Tian, J. Li, P. Ren, X. Bao, Triggering the electrocatalytic hydrogen evolution activity of the inert two-dimensional MoS_2 surface via single-atom metal doping, Energy Environ. Sci. 8 (5) (2015) 1594–1601.
[24] R. Bose, Z. Jin, S. Shin, S. Kim, S. Lee, Y.-S. Min, Co-catalytic effects of CoS_2 on the activity of the MoS_2 catalyst for electrochemical hydrogen evolution, Langmuir 33 (2017) 5628–5635.
[25] M.-R. Gao, J.-X. Liang, Y.-R. Zheng, Y.-F. Xu, J. Jiang, Q. Gao, J. Li, S.-H. Yu, An efficient molybdenum disulfide/cobalt diselenide hybrid catalyst for electrochemical hydrogen generation, Nat. Commun. 6 (2015) 5982.
[26] S. Shin, Z. Jin, S.-Y. Ham, S. Lee, D.-S. Shin, Y.-S. Min, Effect of oxygen incorporation in amorphous molybdenum sulfide on electrochemical hydrogen evolution, Appl. Surf. Sci. 487 (2019) 981.
[27] D. Merki, S. Fierro, H. Vrubel, X. Hu, Amorphous molybdenum sulfide films as catalysts for electrochemical hydrogen production in water, Chem. Sci. 2 (7) (2011) 1262–1267.
[28] J.D. Benck, Z. Chen, L.Y. Kuritzky, A.J. Forman, T.F. Jaramillo, Amorphous molybdenum sulfide catalysts for electrochemical hydrogen production: insights into the origin of their catalytic activity, ACS Catal. 2 (9) (2012) 1916–1923.
[29] S. Shin, Z. Jin, D.H. Kwon, R. Bose, Y.-S. Min, High turnover frequency of hydrogen evolution reaction on amorphous MoS_2 thin film directly grown by atomic layer deposition, Langmuir 31 (2015) 1196–1202.
[30] F. Xi, P. Bogdanoff, K. Harbauer, P. Plate, C. Höhn, J. Rappich, B. Wang, X. Han, R. van de Krol, S. Fiechter, Structural transformation identification of sputtered amorphous MoS_x as an efficient hydrogen-evolving catalyst during electrochemical activation, ACS Catal. 9 (2019) 2368–2380.
[31] H. Shi, X. Fu, X. Zhou, D. Wang, Z. Hu, A low-temperature extraction-solvothermal route to the fabrication of micro-sized MoS_2 spheres modified by Cyanex 301, J. Solid State Chem 179 (2006) 1690–1697.
[32] M. Haruta, J. Lemaitre, F. Delannay, B. Delmon, Preparation and properties of colloidal spherical particles of molybdenum and cobalt sulfides, J. Colloid Interface Sci. 101 (1) (1984) 59–71.
[33] S.B. Maldonado-Zagal, P.J. Boden, Hydrolysis of elemental sulphur in water and its effect on the corrosion of mild steel, Br. Corrosion J. 17 (3) (1982) 116–120.
[34] L. Zhang, J.C. Yu, M. Mo, L. Wu, Q. Li, K.W. Kwong, A general solution-phase approach to oriented nanostructured films of metal chalcogenides on metal foils,, J. Am. Chem. Soc. 126 (26) (2004) 8116–8117.
[35] Y. Hu, Z. Zheng, H. Jia, Y. Tang, L. Zhang, Selective synthesis of FeS and FeS_2 nanosheet films on iron substrates as novel photocathodes for tandem dye-sensitized solar cells, J. Phys. Chem. C 112 (2008) 13037–13042.
[36] S. Oana, H. Ishikawa, Sulfur isotopic fractionation between sulfur and sulfuric acid in the hydrothermal solution of sulfur dioxide, Geochem. J. 1 (1966) 45–50.
[37] A.J. Ellis, W. Giggenbach, Hydrogen sulphide ionization and sulphur hydrolysis in high temperature solution, Geochem. Cosmochim. Acta 35 (1971) 247–260.
[38] P. Walker, W.H. Tarn, Handbook of Metal Etchants, CRC Press, 1991, p. p 823.
[39] B. Schonfeld, J.J. Huang, S.C. Moss, Anisotropic mean-square displacements (MSD) in single crystals of 2H- and 3R-MoS_2, Acta Crystallogr. Sect. B 39 (4) (1983) 404–407.
[40] J.L. Verble, T.J. Wieting, Lattice mode degeneracy in MoS_2 and other layer compounds, Phys. Rev. Lett. 25 (6) (1970) 362–365.
[41] Z. Jin, S. Shin, D.H. Kwon, S.-J. Han, Y.-S. Min, Novel chemical route for atomic layer deposition of MoS_2 thin film on SiO_2/Si substrate, Nanoscale 6 (2014) 14453–14458.

[42] C. Lee, H. Yan, L.E. Brus, T.F. Heinz, J. Hone, S. Ryu, Anomalous lattice vibrations of single- and few-layer MoS_2, ACS Nano 4 (5) (2010) 2695–2700.
[43] B. Meyer, Elemental sulfur, Chem. Rev. 76 (3) (1976) 367–388.
[44] D.H. Kwon, Z. Jin, S. Shin, W.-S. Lee, Y.-S. Min, A comparative study on atomic layer deposition of molybdenum sulfide for electrochemical hydrogen evolution,, Nanoscale 8 (2016) 7180–7188.
[45] J.F. Moulder, W.F. Stickle, P.E. Sobol, K.D. Bomben, Handbook of X-ray Photoelectron Spectroscopy, Perkin-Elmer Co, 1995.
[46] L. Benoist, D. Gonbeau, G. Pfister-Guillouzo, E. Schmidt, G. Meunier, A. Levasseur, XPS analysis of lithum intercalation in thin films of molybdenum oxysulfides, Surf. Interface Anal. 22 (1994) 206–210.
[47] J.O.M. Bockris, A.K.N. Reddy, Modern Electrochemistry, first ed., Plenum Press, New York, 1970, p. p 1242.
[48] R. Bose, S.K. Balasingam, S. Shin, Z. Jin, D.H. Kwon, Y. Jun, Y.-S. Min, Importance of hydrophilic pretreatment in the hydrothermal growth of amorphous molybdenum sulfide for hydrogen evolution catalysis, Langmuir 31 (2015) 5220–5227.
[49] Y. Deng, L.R.L. Ting, P.H.L. Neo, Y.J. Zhang, A.A. Peterson, B.S. Yeo, Operando Raman spectroscopy of amorphous molybdenum sulfide (MoS_x) during the electrochemical hydrogen evolution reaction: identification of sulfur atoms as catallytically acitve sites for H^+ reduction, ACS Catal. 6 (2016) 7790–7798.
[50] B. Seo, S.H. Joo, Recent advances in unveiling active sites in molybdenum sulfide-based electroctalysts for the hydrogen evolution reaction, Nano Convergence 4 (2017) 19.
[51] H. Tributsch, J.C. Bennett, Electrochemistry and photochemistry of MoS_2 layer crystals. I, J. Electroanal. Chem. 81 (1) (1977) 97–111.
[52] N. Pentland, J.O. Bockris, E. Sheldon, Hydrogen evolution reaction on copper, gold, molybdenum, palladium, Rhodium, and Iron: mechanism and measurement technique under high purity conditions, J. Electrochem. Soc. 104 (3) (1957) 182–194.

Supporting Information

Preparation of MoS_2 spheres from Mo plate and elemental sulfur and the effect of sphericalization on electrochemical hydrogen evolution catalysis

Da-Som Shin, Zhenyu Jin, Seokhee Shin, Suhyun Lee, Hyeri Choi, and Yo-Sep Min*

Department of Chemical Engineering, Konkuk University, 120 Neungdong-Ro, Gwangjin-Gu, Seoul 05029, Korea

* ysmin@konkuk.ac.kr

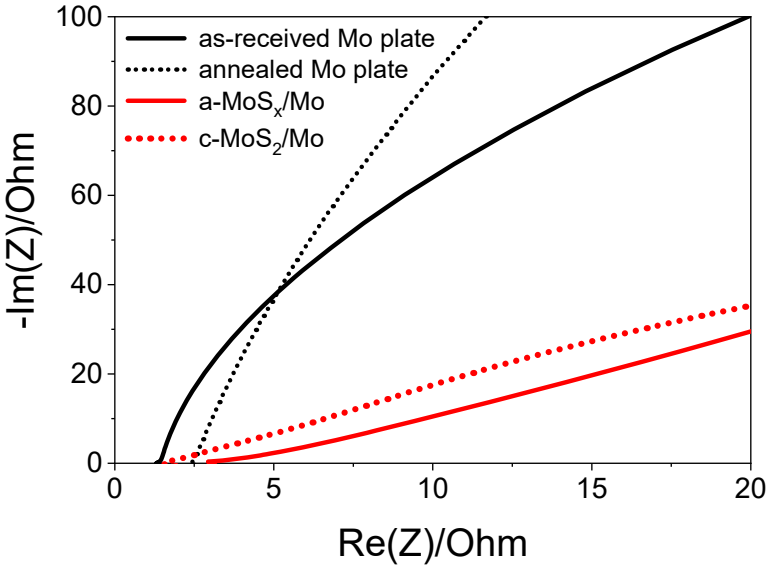

Figure S1. Nyquist plots of as-received Mo plate, annealed Mo plate, a-MoS_x/Mo plate, and c-MoS_2/Mo plate performed at open circuit potential from 200 kHz to 50 mHz, using an AC amplitude of 25 mV.

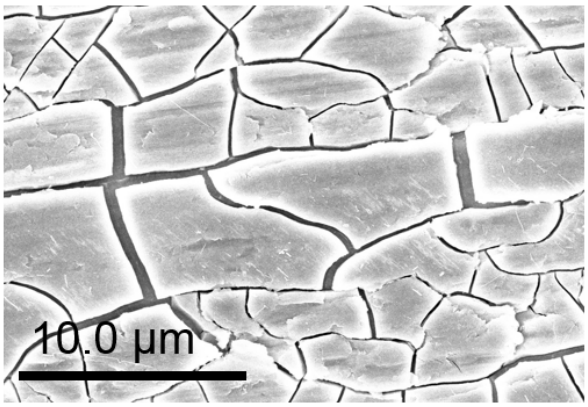

Figure S2. FE-SEM image of Mo plate after the hydrothermal process in a 0.5 M H_2SO_4 solution without any elemental sulfur powder.

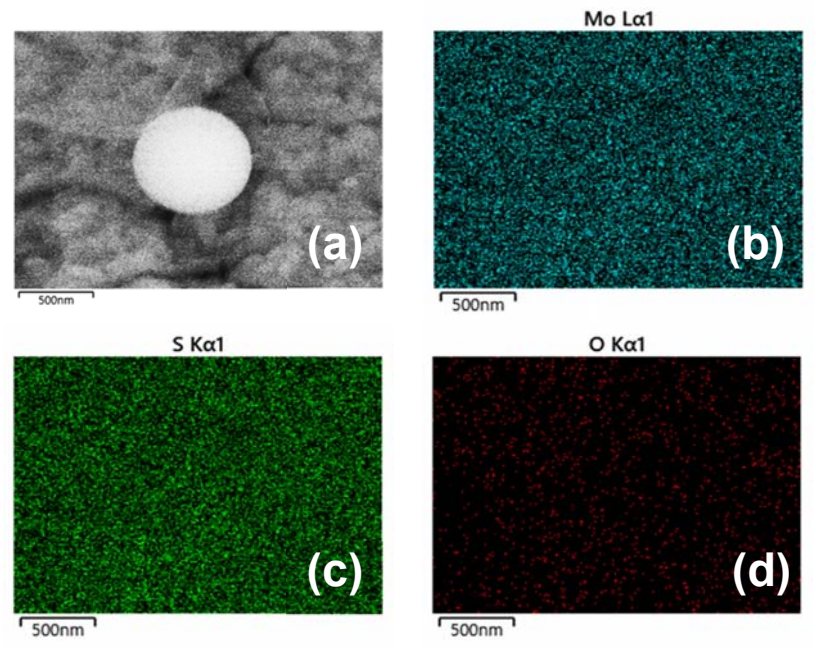

Figure S3. SEM image (a) and EDS mapping images (b-d) of a-MoS_x sphere on a Mo plate: Mo peak (Lα: 2.293 keV), S peak (Kα: 2.307 keV), O peak (Kα: 0.525 keV).

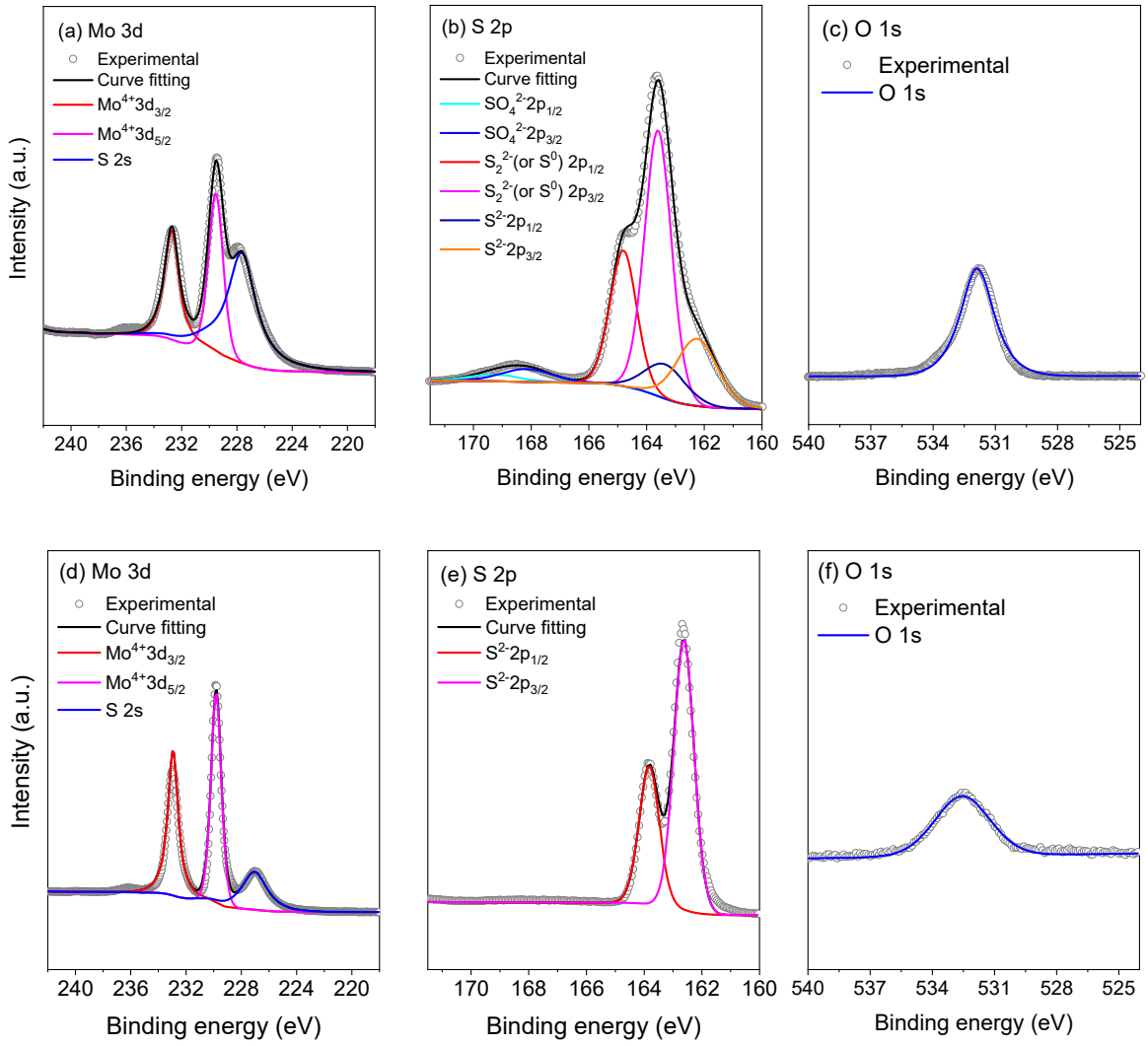

Figure S4. Deconvoluted XPS spectra of a-MoS_x (a-c) and c-MoS_2 (d-f) spheres on Mo plate.

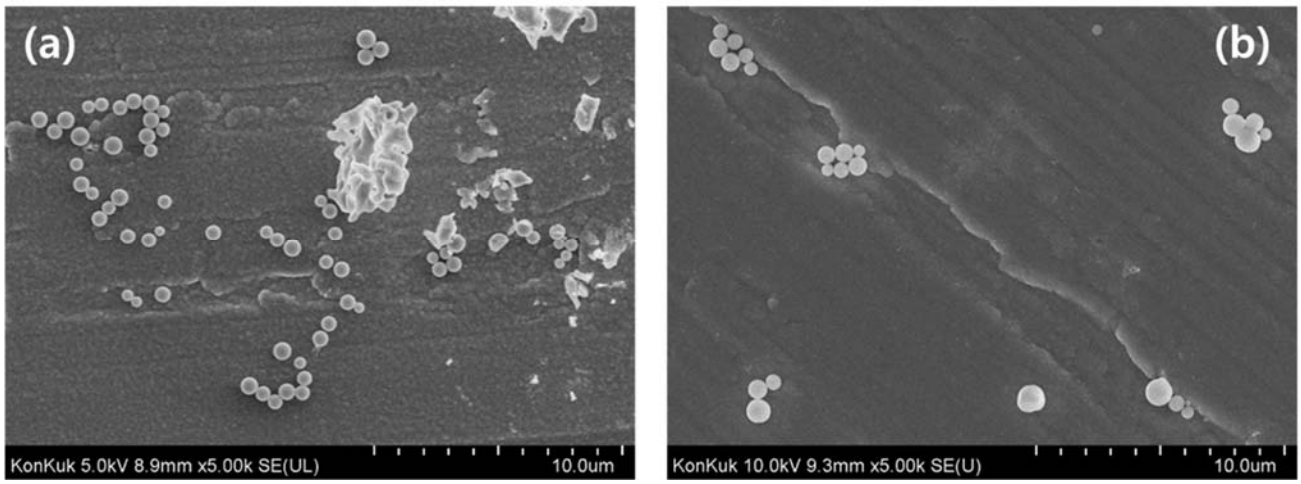

Figure S5. SEM images of a-MoS_x spheres on Mo plates before (a) and after (b) stability test (1000 cycles).

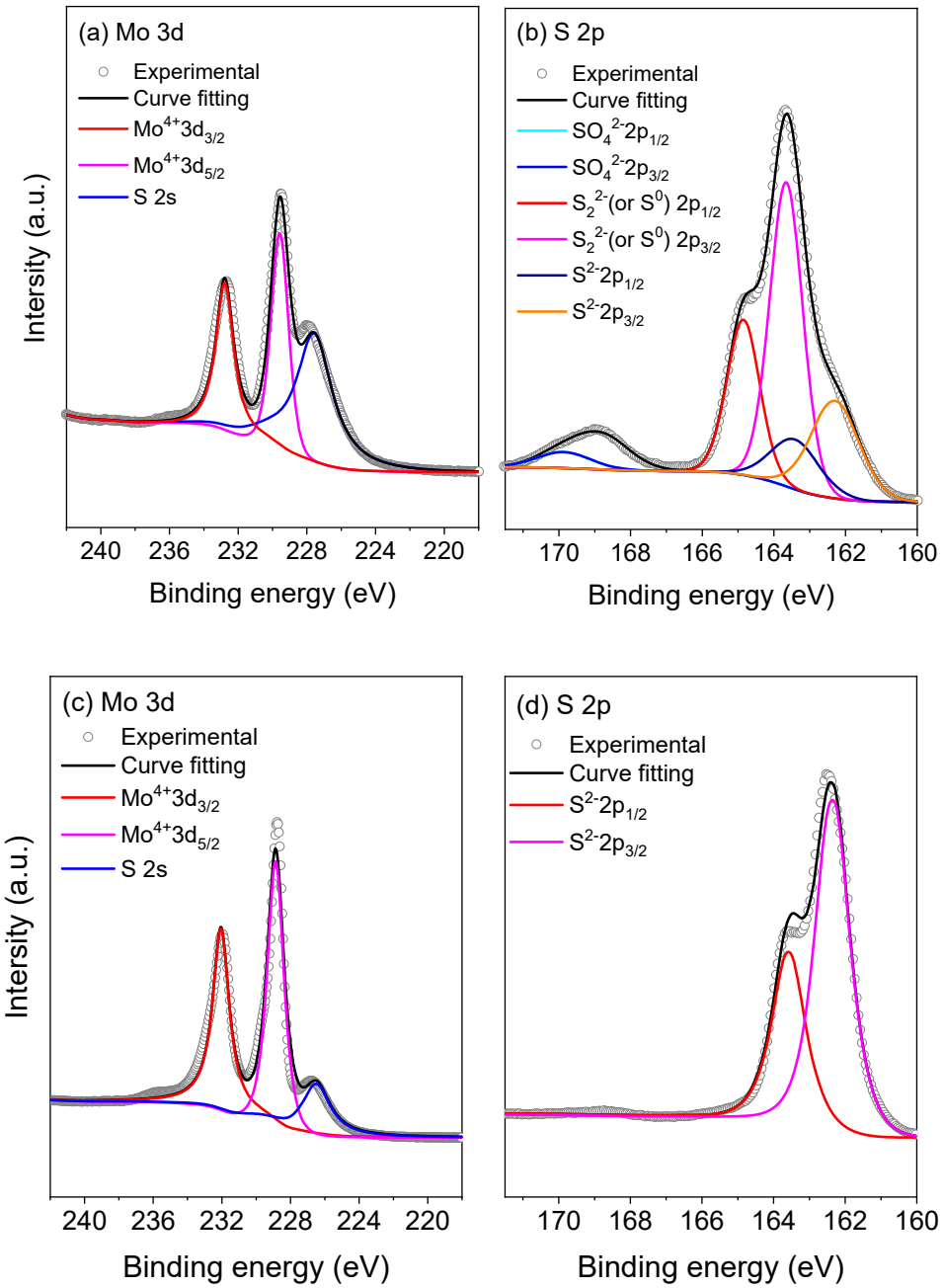

Figure S6. XPS spectra of a-MoS_x/Mo (a, b) and c-MoS_2/Mo (c, d) catalysts after stability test (1000 cycles).

Table S1. The atomic composition of a-MoS_x and c-MoS_2 spheres determined using the deconvoluted XPS spectra

Elements	Atomic composition (%)	
	a-MoS_x	c-MoS_2
Mo^{4+}	9.5	29.5
S^{2-}	19.0	59.4
S^0 (or S_2^{2-})	49.3	-
SO_4^{2-}	4.6	-
O^{2-}	17.6	11.1